A fully manipulable damped driven harmonic oscillator using optical levitation

Javier Tello Marmolejo, Oscar Isaksson, Remigio Cabrera-Trujillo, Niels C. Giesselmann, and Dag Hanstorp

Citation: American Journal of Physics **88**, 490 (2020); doi: 10.1119/10.0000960
View online: https://doi.org/10.1119/10.0000960
View Table of Contents: https://aapt.scitation.org/toc/ajp/88/6
Published by the American Association of Physics Teachers

A fully manipulable damped driven harmonic oscillator using optical levitation

Javier Tello Marmolejo[a)]
Department of Physics, University of Gothenburg, SE-412 96 Gothenburg, Sweden and Facultad de Ciencias, Universidad Nacional Autónoma de México, Ciudad de México 04510, Mexico

Oscar Isaksson
Department of Physics, University of Gothenburg, SE-412 96 Gothenburg, Sweden

Remigio Cabrera-Trujillo[b)]
Instituto de Ciencias Físicas, Universidad Nacional Autónoma de México, Ap. Postal 43-8, Cuernavaca, Morelos 62251, Mexico

Niels C. Giesselmann
Department of Physics, University of Gothenburg, SE-412 96 Gothenburg, Sweden and Physics Institute, Johannes Gutenberg University Mainz, Saarstrasse 21, 55122 Mainz, Germany

Dag Hanstorp
Department of Physics, University of Gothenburg, SE-412 96 Gothenburg, Sweden

(Received 22 October 2019; accepted 25 February 2020)

We implement an experimental system based on optical levitation of a silicone oil droplet to demonstrate a damped driven harmonic oscillator. The apparatus allows us to control all the parameters present in the differential equation that theoretically describes such motion. The damping coefficient and driving force can be manipulated *in situ* by changing the pressure in the apparatus and by applying a variable electric field. We present two different experimental procedures. First, a transition from the overdamped to underdamped regimes is demonstrated by gradually lowering the air pressure. The characteristic resonance associated with an underdamped driven harmonic oscillator is observed by studying how the amplitude of the oscillation varies as a function of the driving force. Second, in order to observe qualitative differences between the overdamped and underdamped regimes of a harmonic oscillator, three driving functions (sine, square, and sharp delta pulses) were separately applied, both at atmospheric pressure and under vacuum conditions. Our overall aim is to design a hands-on apparatus that is easy to use and that allows undergraduate and graduate students to observe and manipulate the basic physical processes associated with a damped driven harmonic oscillator.
https://doi.org/10.1119/10.0000960

I. INTRODUCTION

Oscillatory motion is of great importance in the teaching of physics at all levels. For example, it appears in textbook subjects such as mechanics, electromagnetism, and waves. Traditionally, oscillatory motion is introduced to undergraduate students by using the simple pendulum or a mass-spring system. In such simple cases, the equation of motion can be easily solved since the restoring force is proportional to the displacement, i.e., it obeys Hooke's law. Both the ideal undamped oscillator and the more realistic damped oscillator are described by a second-order differential equation that admits closed analytical solutions.[1,2] Such a system is referred to as a harmonic oscillator (HO). There are many diverse applications involving HOs, including the Laser Interferometer Gravitational-Wave Observatory (LIGO) search for gravitational waves,[3] nonlinear driven oscillations of the string of a guitar,[4] motion of ultracold atoms in a harmonic trap,[5] laser cooling of atoms,[6] and medical-physics studies of the human body's response to glucose.[7]

A harmonic oscillator subjected to driving and damping forces is referred to as a damped driven harmonic oscillator (DDHO). This system is commonly used in physics as a model to study resonance phenomena.[1,8] Such phenomena occur in many fields of science and engineering,[2,9] for example, subatomic particle resonances,[10] design of picogram mass sensors,[11] and energy cost calculations of human walking.[12] Nevertheless, a short sampling of physics textbooks[13–16] shows that most of the DDHO-related examples are limited to springs, pendulums, or electronic circuits.[8,9,17] Springs have the advantage that they are visible and suitable for demonstrations, but their damping forces are difficult to vary. On the other hand, parameters are easy to change in electric circuits, but the effects they produce are not directly observable. Finally, in pendulums, harmonic oscillator approximation is not valid for large amplitude oscillations, and the resonance condition must be calculated numerically.[18] For these reasons, visible demonstrations of resonance behavior are difficult to achieve.

Often, students first observe evidence of a resonance in a video of a drinking glass being shattered by a sound wave or a bridge collapsing as a result of mechanical vibrations. However, optical manipulation (OM) offers a different approach to the study of oscillations and resonances. Here, a focused laser is used to trap small particles in a harmonic potential well. The movement of the particle is described by the DDHO differential equation, where the main parameters are the restoring force constant, the damping coefficient, and the driving force. OM presents a visible approach to the study of the motion of a DDHO for which the main parameters can be easily varied.

The use of laser light to manipulate microscopic objects was first demonstrated in the 1970s by Arthur Ashkin and Joe Dziedzic.[19] They discovered how to exert forces on micron-sized particles using continuous-wave laser beams. In 1971, these authors were able to levitate several glass spheres,[20] initiating the field of optical manipulation, where the main tools are called optical tweezers. Today, trapping and manipulating small particles have developed into an important research technique and, as a consequence, Arthur Ashkin was awarded the Nobel Prize in 2018. The educational uses of OM that appear in the literature are ample. Designs for cheap optical tweezers systems have been reported[21–23] with applications to biophysical educational modules[24] as well as demonstrations of the interaction of ionizing radiation with matter.[25] Useful resources, such as a theoretical approach for undergraduates[23] and downloadable trapping simulation software,[26] are also available.

Optical levitation under vacuum conditions was also introduced by Ashkin *et al.*[27] in experiments, where the underdamped harmonic oscillation of a levitated droplet was observed. In the present work, we extend these pioneering experiments to an investigation of resonance behavior associated with the motion of a levitating droplet. We also show the transition between the overdamped and underdamped regimes and make a comparison of the oscillator's characteristic parameters in each case.

With this purpose in mind, a versatile optical levitation system has been developed in which the three parameters in the DDHO differential equation are fully manipulable. The driving force and damping coefficient can be manipulated *in situ* by varying the air pressure in the trapping chamber and the magnitude of the applied electric field. The restoring force constant, commonly known as trap stiffness in the OM field, can be varied by changing the focal length of the lens that focuses the laser to form the trap. In this manner, we were able to create an oscillator and have control over all the parameters in the DDHO equation.

Two experiments are presented, whose results can be recorded in a computer, magnified for view on a screen, or viewed with the naked eye. In the first experiment, a droplet is trapped at different pressures and made to oscillate in the presence of a sinusoidal driving electric force. The transition from the overdamped to underdamped regimes can be observed at a critical pressure value of about 1 mbar. Below this value, resonance begins to appear. Students are then able to measure the resonance frequency empirically and use it to calculate the restoring force constant of the system.

In the second experiment, students observe qualitative differences between the overdamped and underdamped regimes by driving the droplets in both regimes at atmospheric pressure as well as under vacuum conditions with sine, square, or sharp delta pulse functions. The results are in agreement with the known theoretical results found in the literature.

Our system offers undergraduate or graduate physics students an easily understandable approach, which connects the fields of mechanics, optics, and fluid dynamics. At the same time, it introduces students to the topic of optical manipulation, which is widely used in modern research fields.

Our work is presented in the following manner. In Sec. II, we briefly describe the fundamentals of DDHO theory. In Sec. III, we present the design of our experimental setup, and in Sec. IV, we discuss our findings and provide a discussion of these results. Finally, in Sec. V, we give the conclusions derived from our work.

II. THEORY

A. Damped driven harmonic oscillator

The motion of a droplet trapped in a harmonic potential well, driven by an external force and damped by the air, is governed by the DDHO equation

$$\frac{d^2y}{dt^2} + \gamma\frac{dy}{dt} + \omega_0^2 y = \frac{F}{m}, \tag{1}$$

where y is the vertical position of the droplet with respect to its equilibrium position, γ is the air friction coefficient, ω_0 is the angular resonance frequency, F is the driving force, and m is the mass of the particle. The resonance frequency ω_0 is related to the restoring force constant k by the equation

$$\omega_0^2 = \frac{k}{m}. \tag{2}$$

For a given resonance frequency ω_0, the particle will be in either the overdamped or the underdamped regime, depending on the magnitude of the air friction coefficient γ given by the expressions

$$\begin{aligned} &\gamma^2 - 4\omega_0^2 > 0 \quad \text{overdamped},\\ &\gamma^2 - 4\omega_0^2 < 0 \quad \text{underdamped}. \end{aligned} \tag{3}$$

There is a significant qualitative difference between these two regimes. Figure 1 shows the theoretical response of a particle displaced from the stability position for both overdamping and underdamping. In the overdamped regime [Fig. 1(a)], the return to equilibrium is exponential in time while, for underdamping [Fig. 1(b)], the return is the product of a sinusoidal oscillation and a decaying exponential.

Another important difference between these two regimes is the enhancement in amplitude of the resonance when the damping is small. Solving the DDHO differential equation [Eq. (1)] for a sinusoidal driving force $F = F_0 \sin(\omega t)$ gives

$$y = A(\omega, \gamma)\sin(\omega t - \alpha), \tag{4}$$

where ω is the driving frequency. The phase shift α between the driving force and the oscillator is given by[13,28]

$$\alpha(\omega, \gamma) = \frac{\pi}{2} - \arctan\left(\frac{\omega^2 - \omega_0^2}{\gamma\omega}\right), \tag{5}$$

while the oscillation amplitude A is[13,28]

$$A(\omega, \gamma) = \frac{F_0}{m}\frac{\sin\left(\frac{\pi}{2} + \alpha\right)}{\omega_0^2 - \omega^2}. \tag{6}$$

Figure 2 shows curves derived using Eqs. (5) and (6). These curves represent the amplitude of the oscillation as a function of the driving frequency ω, where each curve is plotted for a different value of the damping constant γ. The assumed numerical value of γ is indicated below each curve. Close to the vertical line in Fig. 2(a), a gradual increase in amplitude with respect to frequency can be observed. This increase is only apparent in the underdamped regime and is represented by the curves above the critical case, i.e., the curves for $\gamma = 1$ and $\gamma = 0.4$.

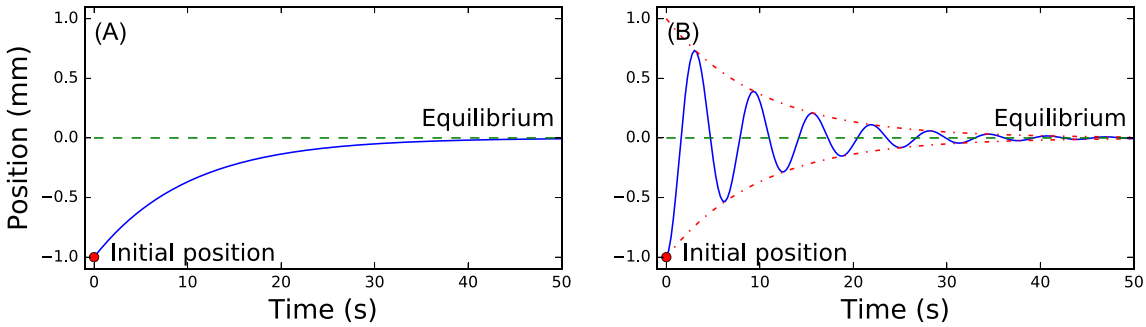

Fig. 1. (Color online) Theoretical temporal return to the equilibrium position of a displaced particle in an (a) overdamped and (b) underdamped harmonic oscillator. The dot-dashed curve in (b) is plotted to show the exponential decay of the oscillations.

B. Stokes' law

A spherical droplet moving (at sufficiently slow speed) in air experiences a damping force F_d due to friction given by Stokes' law[14]

$$F_d = 6\pi\eta r v, \tag{7}$$

where η is the viscosity of air, r is the radius of the droplet, and v is the speed of the particle. The $6\pi\eta r$ term corresponds to the air friction coefficient γ defined previously. As air pressure is decreased, air viscosity and, along with it, air friction are reduced. For droplets with a diameter of around 20 μm, like the ones presented here, air pressures below 1 mbar are required to bring the motion into the underdamped regime.

Equation (7) implies that the air around the droplet is in laminar flow, that is, the Reynolds number is small. For a sphere moving in air, Reynolds number is defined as $R_e = \rho d v/\eta$, where ρ is the density of air, d is the droplet diameter, v is the air velocity respect to the droplet, and η is the viscosity of air. Using standard values at normal temperature and pressure (NTP), $\rho = 1.28$ Kg m^{-3}, $\eta = 1.83 \times 10^{-5}$ N s m^{-2}, $d = 20 \times 10^{-5}$ m. Then, for a sphere with velocity $v = 0.05$ m/s, we obtain $R_e \approx 0.07$. The values given here represent the largest velocity and density of the air, respectively, in our experiment. Hence, all data shown in this work have been obtained with a droplet moving in the laminar regime.

C. Optical levitation

An optical levitation trap for spherical droplets consists of a laser beam directed upwards and focused by a lens, as shown in Fig. 3. Here, we assume that we are in the ray optics regime, since all the dimensions in the experiment are much larger than the wavelength of the laser light. The laser light can then be considered as individual rays that carry momentum. When laser light is absorbed, refracted, or reflected by a droplet in the trap, there is a transfer of momentum to the droplet. This momentum transfer creates a vertical force, termed the *scattering force*, given by[29]

$$F_{\text{scatter}} = Q\frac{nP}{c}, \tag{8}$$

which pushes the droplet in the direction of the laser beam. Here, P represents the laser power that strikes the droplet, n is the droplet's refractive index, c is the speed of light, and Q is a dimensionless factor between 0 and 2. If all of the light is reflected, $Q = 2$; if it is all absorbed, $Q = 1$; if it is all transmitted, $Q = 0$.

As the droplet falls closer to the laser beam waist, the beam profile becomes narrower, increasing the optical power density and, with it, the magnitude of the scattering force. At equilibrium, the upward-directed scattering force is exactly equal to the downward-directed gravitational force, creating a stable trapping position along the beam axis. Above this stable point, the net force pulls the droplet down; below it, the droplet is pushed up. The droplet is trapped in the region above the focal point in a Gaussian beam waist, where the size of the beam is increasing linearly with the vertical position. By integrating the Gaussian profile over the size of the droplet, one can show that the amount of light that strikes the spherical droplet varies linearly, as it moves along this laser profile. We have also experimentally confirmed that the

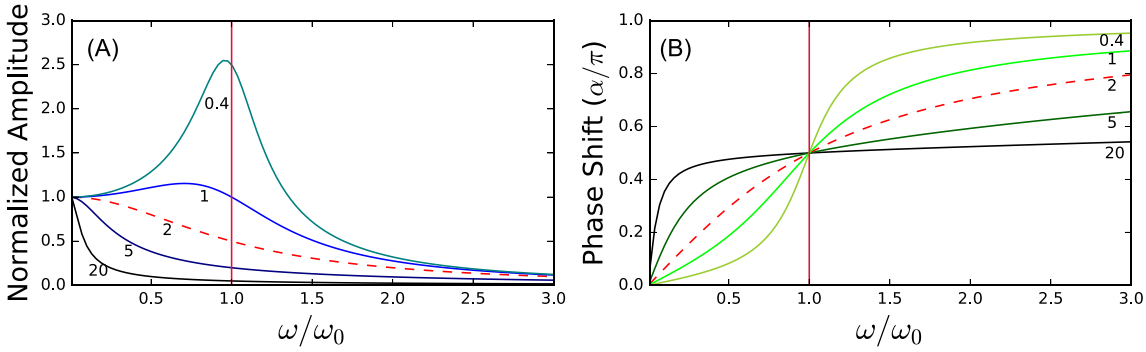

Fig. 2. (Color online) Calculated (a) amplitude and (b) phase shift, as a function of the driving frequency for a DDHO. The dashed curve shows the critically damped case. The numbers below the curves indicate the values of the frictional damping coefficient γ. The vertical solid lines mark the resonance frequency.

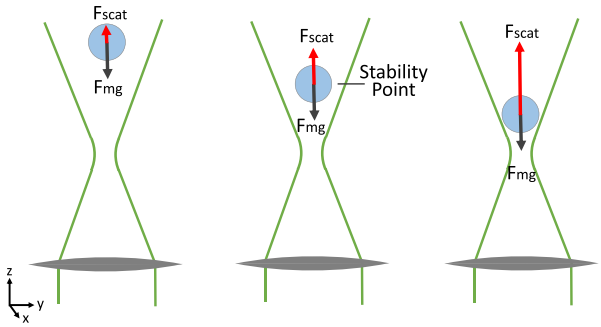

Fig. 3. (Color online) At the equilibrium (stability) point for the spherical droplet, the scattering force cancels out the gravitational force. When displaced, the droplet is pushed back towards the stability point via a harmonic restoring force.

restoring force is linear as the droplet is moved away from the equilibrium point. Hence, we have a harmonic trap in the vertical direction.

A restoring force also exists in the radial direction. A droplet displaced from the center of a Gaussian laser profile beam, as shown in Fig. 4, refracts more light towards the direction it is displaced. To conserve momentum, the droplet experiences a force in the opposite direction to its displacement. This force is called the *gradient force*. The scattering and gradient forces together establish a stable trapping point in space for the droplet.

D. A charged particle in an electric field

The droplets used in our experiments are negatively charged (as will be discussed in Sec. III) and can hence be manipulated with electrical fields. In the centre of the ringed electrodes, a locally homogeneous vertical electric field is created. This can be approximated as a set of two horizontal plane electrodes, and the magnitude of the field will be given by

$$E = \frac{V}{d}, \tag{9}$$

where V is the applied voltage and d is the distance between the plane electrodes. A droplet with negative charge q placed in such an electric field experiences a force in the opposite direction of the applied field that has a magnitude of

$$F = Eq. \tag{10}$$

Here, $q = -N_e e$, where N_e is the number of excess electrons on the droplet and the electric field E is directed downward for positive voltages.

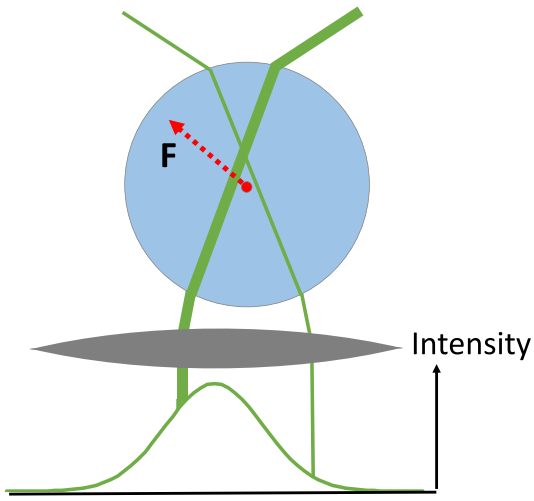

Fig. 4. (Color online) A radially displaced spherical droplet feels a restoring gradient force towards the center of a Gaussian beam.

III. EXPERIMENTAL SETUP

A. Trapping and manipulation

The setup used in this work is shown schematically in Fig. 5(a). A droplet is levitated inside an aluminum vacuum chamber 60 mm high, 50 mm wide, and 50 mm deep. The chamber has a window on the lower face through which the laser beam enters and windows on the sides to let the light scattered from the droplet out. A removable lid on the top surface is used to enclose the system after a droplet is trapped. A detailed list of the components and approximate price is provided in the Appendix.

1. Trapping

In our work, we use a continuous-wave laser at a wavelength of 532 nm. The laser's output power is 2 W, and it produces a Gaussian beam profile (Laser Quantum gem532). The laser beam is directed vertically upwards by use of a mirror and is focused by a 100 mm biconvex lens (Lens 1) into the vacuum chamber. A lens with long focal length was chosen in order to create a somewhat weaker trap in the vertical direction, thus enhancing the driven motion of the droplet in this direction. Our experience shows, however, that lenses with focal length as short as 30 mm also allow successful trapping. The focusing lens is placed about 70 mm below the lower window in order to focus the laser close to the center of the chamber. A liquid microdispenser (GeSiM Bent Steel Capillary) is situated directly above the laser beam and is used to dispense micron-sized droplets into it. The dispenser consists of a capillary attached to a piezoelectric crystal. By applying a voltage to the piezo crystal, a micrometer-sized droplet is emitted. The droplet emitted from the dispenser becomes negatively charged due to friction between the dispenser and the droplet. The emitted droplet falls under gravity into the laser field until it is trapped. A trapped droplet levitates above the focal point and scatters light in all directions. The laser power needed for trapping was in the range of 400–1000 mW. Once a droplet is trapped, the lid is carefully put back into place.

The microdispenser's syringe contains a solution with a 5:1 ratio of isopropanol-to-silicone oil. The isopropanol in a levitated droplet evaporates quickly and only the silicone oil remains. The dispenser produces droplets with very small dispersion in size. According to the manufacturer specifications, the minimum diameter of a dispensed droplet is 55 μm, which shrinks to about 30 μm after the evaporation of the isopropanol. Silicone oil was chosen because of its high vapor pressure, which stops it from evaporating in vacuum. The silicone oil and isopropanol solution were chosen, because its reduced viscosity facilitates the dispensing process.

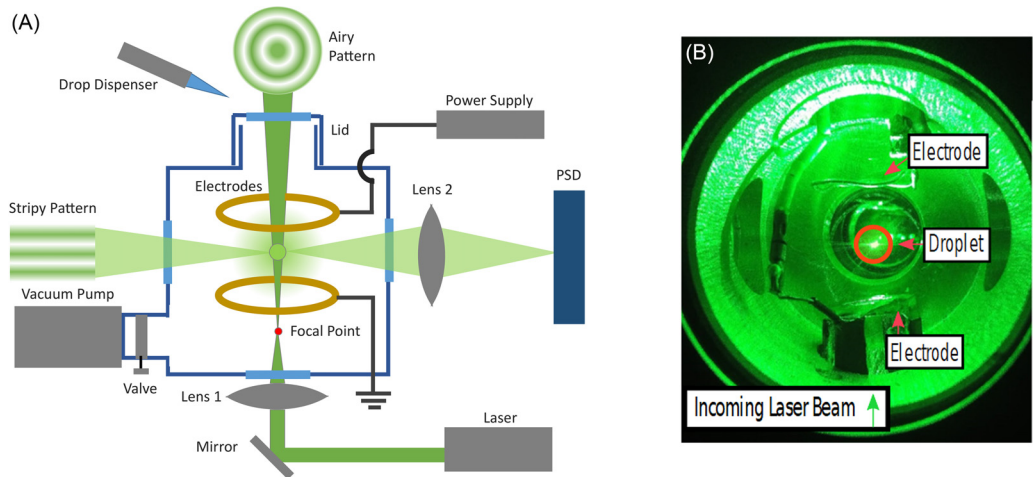

Fig. 5. (Color online) (a) Sketch of the experimental apparatus. Inside a vacuum chamber, a focused laser beam creates an optical levitation trap for a micron-sized silicone oil droplet. The droplet levitates above the focal point of Lens 1; the focal point is indicated by a dot. An illustration of the diffraction patterns produced by the droplet is shown above the apparatus and to its left. The position sensitive detector (PSD) is shown to the right. (b) Photo of the experimental chamber. A levitated droplet is seen as a small bright spot in the center of the image.

2. Manipulation of the air damping

A vacuum pump (Pfeiffer Vacuum DUO5M) is connected to the side of the vacuum chamber through a variable leak valve (Leybold Gmbh DN 16 ISOKF right angle valve). The system pump can be used to reduce the pressure in the chamber from atmospheric pressure to 1×10^{-2} mbar. A pressure gauge (Pfeiffer Single Gauge) measures the air pressure inside the chamber. The air was pumped out slowly to avoid strong air currents inside the chamber that could push the droplet out of the trap. The speed of the pumping is controlled by opening the valve. It takes about 10 min to reduce the pressure to the minimum inside the chamber without losing the droplet.

3. Manipulation of the driving force

Inside the chamber, there are two horizontal ring-shaped electrodes (see Fig. 5). They have a radius of 5 mm and a vertical separation of 20 mm. Hence, the laser beam can pass through the center of the rings without being intercepted. The position of the electrodes inside the chamber is such that the lower one lies above the focal point of Lens 1. The lower electrode is connected to the vacuum chamber, which in turn, is connected to the electrical ground. The upper electrode is connected to a voltage amplifier (Kepco BOP1000M) with a maximum voltage output of ± 1000 V. The power supply is fed with a signal from a function generator (Leader LFG-1300), which can deliver a variety of functions (AC, DC, squared, etc.) with an output voltage in the range of ± 10 V. The amplifier then multiplies the input times 100.

The voltage difference between the electrodes creates a locally homogeneous, vertically directed electric field. This field will, since the droplets carry a negative charge, produce a driving force. The voltage needed to manipulate the droplets depends on their charge and mass, but effects visible to the eye could be achieved with voltage in the range 20 V to 1000 V.

B. Visualization

The technique of recording the vertical displacement of the droplet is very similar to the one that has been presented in detail by Isaksson *et al.*[25] In short, a 30 mm lens (Lens 2), placed 33.6 mm away from the droplet, focuses the scattered light onto a position sensitive detector (PSD) (Sitek Electro Optics AB S10006) situated at a distance of 280 mm from the lens. The PSD is connected to a computer via a data acquisition device (National Instruments BNC-2110 connected with a SCH68–68-EPM cable to a PCIe-6321 placed in an expansion slot of the computer). A custom-made LabVIEW program calculated the droplet's real displacement. However, it is also possible to project a magnified image of the droplet onto a screen or to simply observe its oscillations directly with the naked eye, using appropriate protective goggles.

C. Size measurement

For several applications, it is necessary to know the size and mass of the droplet. The diffraction patterns the droplet creates when situated in the laser beam can be used to measure these parameters with micrometer precision.

Along the direction of the laser, the droplet acts as a circular obstacle around which the reminder of the beam passes. Such an obstacle creates an Airy diffraction pattern [see Fig. 6(a)]. The radius r of the droplet can be determined from the first dark ring's diameter Z by[30]

$$r = 1.22\,\frac{\lambda R_{\text{Airy}}}{Z}, \tag{11}$$

where λ denotes the wavelength of the light and R_{Airy} is the distance between the object and the screen.

The light scattered from the droplet to the sides can be modeled as two bright point sources coming from the top

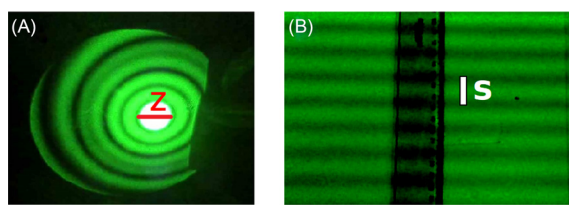

Fig. 6. (Color online) (a) Airy pattern produced by the droplet. The horizontal line marks the diameter Z of the first dark ring. (b) Double-slit diffraction pattern created by a levitated droplet. S is the distance between two dark interference bands.

and bottom of the sphere. This creates a double-slit diffraction pattern [see Fig. 6(b)], where the separation between the two bright sources (slits) is the droplet diameter. S is the distance between the center of two dark lines, and R_{Stripes} is the distance between the droplet and the screen. The radius r of the droplet is given by[31]

$$r = \frac{2\lambda R_{\text{Stripes}}}{S(2+\sqrt{2})}. \tag{12}$$

The mass m of the spherical droplet can then be calculated using the density of silicone oil $\rho = 971\,\text{kg/m}^3$ at 25 °C in the equation

$$m = \rho V = \rho\left(\frac{4}{3}\pi r^3\right). \tag{13}$$

IV. RESULTS AND DISCUSSION

A. Resonance frequency

A sinusoidal driving force was applied to a trapped droplet in air by modulating the magnitude of the electric field. The frequency of the driving force was then slowly increased. Figure 7 shows the resulting oscillations of the droplet (decaying amplitude curve) and the driving force (constant amplitude curve). As to be expected from an oscillator in the overdamped regime, the amplitude of the oscillations decreases as the frequency is increased. Additionally, friction from the air causes a lag in the motion that creates a phase shift. This effect can be seen, for example, at $t = 38\,s$ in Fig. 7, where the crests of the oscillation and the driving motion do not overlap.

A frequency sweep of the driving force, like the one shown in Fig. 7, was repeated at decreasing pressures. For every oscillation, the amplitude and phase shift were determined and plotted against the driving frequency. The amplitudes were normalized to that at the lowest frequency.

Figure 8 shows a gradual transition from the overdamped to the underdamped regimes recorded, when the air pressure inside the chamber was decreased. Each frame shows a frequency sweep at a different air pressure. The effect on the amplitude and phase shift is apparent. The same procedure is followed for other pressures. The circular and triangular symbols represent the experimental data. The amplitude and phase shift curves are obtained by use of Eqs. (6) and (7), respectively. Both equations depend only on the restoring constant and the damping coefficient. These constants were found by fitting Eq. (6) to the experimental amplitude data at each pressure. The same pair of constants were then used to plot both the amplitude and phase shift curves.

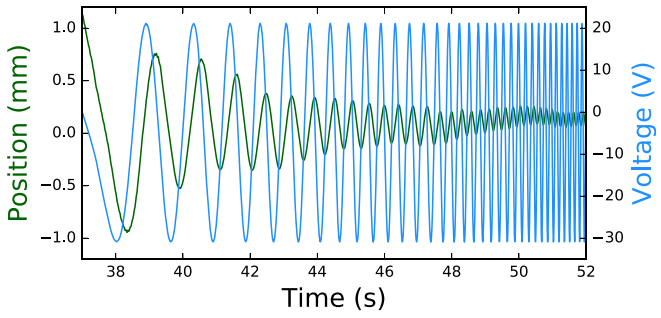

Fig. 7. (Color online) Position of a levitated droplet at air pressure of 980 mbar decaying amplitude curve driven by a sinusoidal force constant amplitude curve.

There are some outlying points in Fig. 8, such as those close to 34 rad/s in Fig. 8(e). These outliers are caused by so-called whispering gallery modes,[32] which occur when the circumference of the droplet exactly matches an integer multiple of the laser wavelength. Under this condition, the optical coupling into the droplet increases, causing a larger scattering force, which in turn changes the force balance that holds the droplet in equilibrium. This circumstance occurs, because the silicon oil is very slowly evaporating, causing a change in the size of the droplet. However, it was found that these outlying points did not affect the fitting of the data to the DDHO model and so no correction was needed. A more detailed discussion of this effect is outside the scope of this paper, and it is left for a forthcoming publication.

By qualitatively comparing Figs. 8 and 2, we can see that at 980 mbar and 8.7 mbar the system is overdamped, at 1 mbar it is critically damped, and below 1 mbar it is underdamped. Furthermore, in the underdamped regime, a resonance starts to appear in the amplitude data. In particular, at 0.3 mbar, one observes a significant 2.5 times increase in the peak amplitude with respect to that at low driving frequencies.

The value of the resonance frequency can be calculated by fitting the data using Eq. (6). Alternatively, one can empirically find the value at which the amplitude is maximized from the experimental data. In Fig. 8(e), the resonance occurred at a driving frequency of $w_0 = 30$ rad/s. The droplet produced an Airy pattern with a diameter of $Z = 7.7 \pm 0.2$ cm. Hence, using Eq. (11), it had a radius of $10.7 \pm 0.2\,\mu$m. Then, using Eq. (13), we find the droplet had a mass of $5.0 \pm 0.2 \times 10^{-12}$ kg. The resulting restoring force constant derived from Eq. (2) is $k = 4.59 \pm 0.16$ nN/m. Calculating the restoring constant using a previous procedure,[25] in which a change in laser power is balanced by the electric field, gave $k = 4.10 \pm 0.60$ nN/m.

At the resonance frequency $\omega_0 = 30$ rad/s, the phase shift between the driving field and the position of the droplet is $\pi/2$. As a consequence, the velocity of the droplet, which is the derivative of its position, is in phase with the sinusoidally varying electric field. Thus, the force is always pushing the droplet in the direction of its velocity and, as a consequence, increases the amplitude of the oscillation.

B. Overdamped and underdamped regimes

To investigate other qualitative differences between the overdamped and underdamped regimes, a droplet was trapped in air as well as in near-vacuum conditions, and driving functions with different time structures were applied. Results of this investigation are shown in Fig. 9. The time-dependent position of the droplets is shown by the solid green curves, and the dashed blue curves represent time dependence of the applied driving force. A function generator was used to produce the following driving forces: (a) sinusoid at atmospheric pressure, (b) sinusoid at near-vacuum (10^{-2} mbar), (c) square pulsed function with a time width of 5 s at atmospheric pressure, and (d) sharp delta pulse at near-vacuum.

In the case of a sinusoidal driving force in air at atmospheric pressure, the damping due to friction reduces the amplitude of the oscillation and creates a phase lag between the value of the driving force and the position of the droplet. The phase lag is barely present in the case of near-vacuum, where frictional damping is negligible. This qualitative

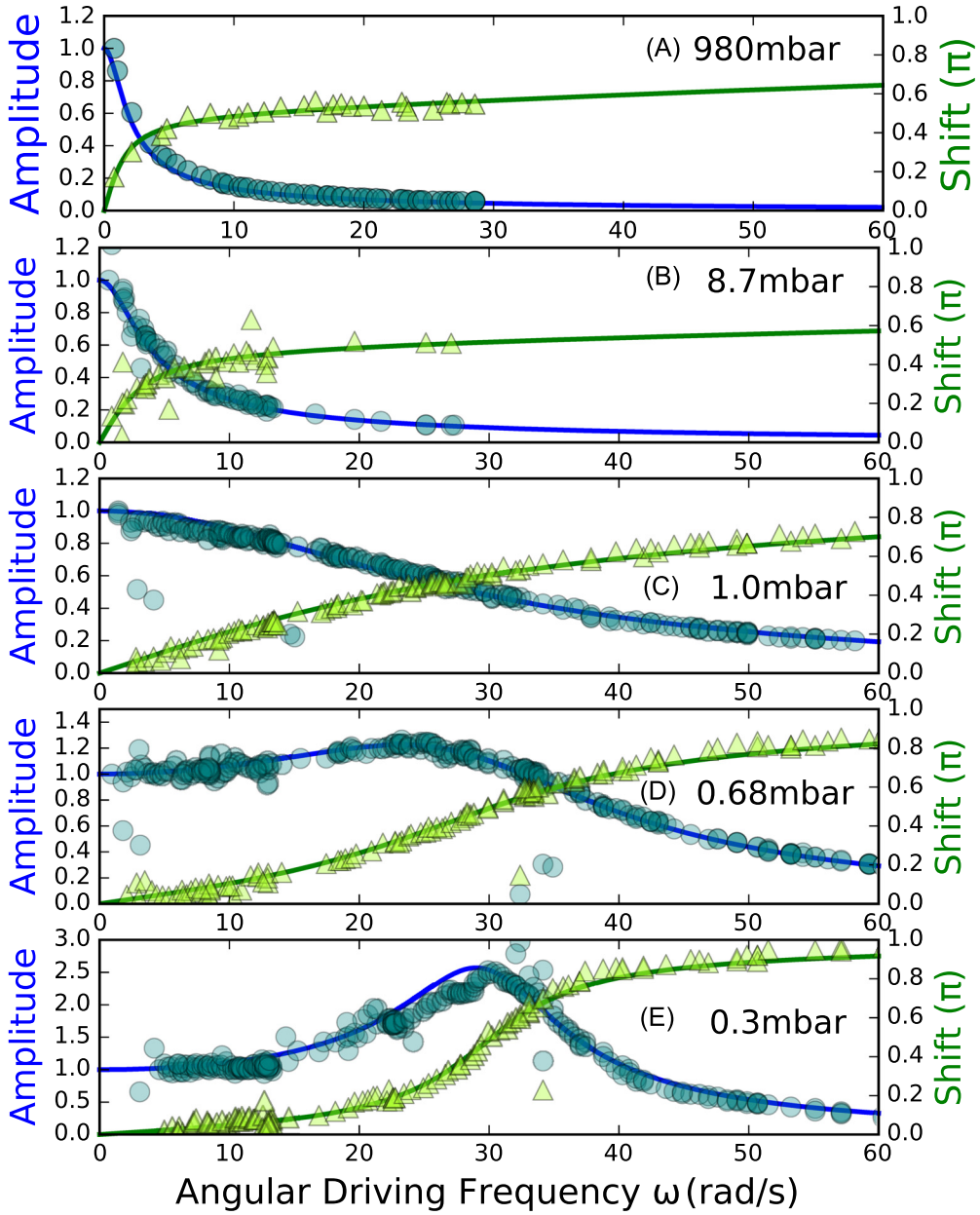

Fig. 8. (Color online) Gradual transition between the overdamped and underdamped regimes of an optically levitated droplet at five different pressures. (a) and (b) show the overdamped regime; (c) represents a critically damped system; and (d) and (e) represent the underdamped regime. In the underdamped regime, a resonance structure begins to appear. The circular experimental data symbols (○) represent the normalized amplitude of each oscillation, and those shown as triangles (△) represent the measured phase shift. The pressure was maintained constant throughout each frequency sweep. The figure also shows some outlier points, such as those at 34 rad/s in (e), which are caused by the so-called Whispering Gallery modes; see the text for discussion.

difference is shown in Figs. 9(a) and 9(b), where the dotted vertical lines mark the crests of the two functions. The distance between the vertical lines represents the phase shift. It can be seen that below 1 mbar, the phase shift is close to zero because the drag caused by the air is significantly reduced. In contrast, at atmospheric pressure, the frictional drag force produces a larger phase shift and a reduction in amplitude compared to the same quantities under vacuum conditions.

Another qualitative comparison can be made between Figs. 9(c) and 9(d). In Fig. 9(c), a slowly varying square pulse driving force was applied at atmospheric pressure. The frictional damping, at this air pressure, slows down the droplet and its return to equilibrium, after the driving force is removed, has an exponential behaviour, as shown in Fig. 1(a). In Fig. 9(d), a sharp delta pulse driving force momentarily displaced the droplet when in near-vacuum. With small frictional damping under the near-vacuum conditions, the droplet returns to the equilibrium position, and an oscillation around this point followed. The amplitude of the oscillations decrease exponentially as the droplet is slowed down by the frictional interaction with the air. Additional curves are plotted to show the exponential decay of the amplitude of the oscillator. This behavior coincides qualitatively with the one displayed in Fig. 1.

V. CONCLUSIONS

The motivation for the present work was to create an easily visualizable damped driven harmonic oscillator, which

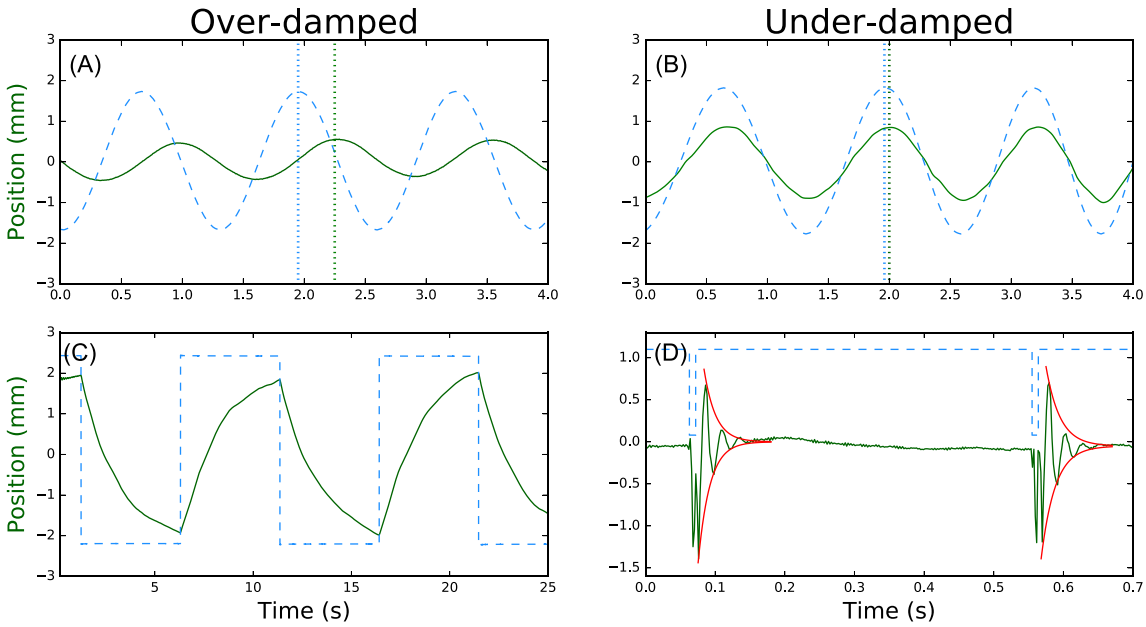

Fig. 9. (Color online) Comparison of the behavior of levitated droplets' position (solid curve) in the over-damped and under-damped regimes for different time-structures of the applied electrical force (dashed curve). (a) Sinusoidal driving force in air at atmospheric pressure (980 mbar). The damping reduces the amplitude and causes a phase shift between the two curves. The dotted vertical lines mark the crests of the driving force (dotted vertical line) and the droplet's position (dotted line). (b) Sinusoidal driving force at near-vacuum (1×10^{-2} mbar air pressure). In near-vacuum, the frictional damping is negligible. The amplitude is larger than it was at 980 mbar and the phase shift between the curves is close to zero. (c) Pulsed square function driving force in air at atmospheric pressure. The motion to the new equilibrium position after the driving force is removed follows a decaying exponential function. (d) Sharp delta pulse in near vacuum (1×10^{-2} mbar). The return to equilibrium is oscillatory since damping has been greatly reduced. Additional curves are drawn to show the exponential decay of the amplitude.

will allow instructors to introduce the concept of a mechanical resonance to students. Such a system is described theoretically by a second-order differential equation with frictional damping, resonance frequency, mass, and frequency and amplitude of the driving force as its parameters. The goal was achieved by building an optical levitation apparatus that allows us to experimentally manipulate these parameters and, at the same time, introduce students to optical manipulation.

By changing the pressure inside the vacuum chamber and thereby changing the amount of frictional damping, we were able to observe the transition between the overdamped and underdamped regimes of the DDHO. In particular, in the underdamped regime, a broad resonance was observed in the oscillation data over a range of frequencies of the sinusoidal driving force.

We were also able to show how the temporal structure of the driving force could be changed by using a function generator. We used sine, square, and sharp delta pulse functions in the experiment, but in general, any function could be applied. The response to the applied driving forces was shown to be in agreement with theory, and the results were used to compare the overdamped and underdamped regimes of the DDHO.

The apparatus is such that students can easily manipulate the driving force and friction coefficient by just turning associated "knobs." It was very satisfying for us to see how such a simple apparatus can be used to illustrate the physics of a damped driven harmonic oscillator. The apparatus showcases oscillatory behavior in optics, fluid dynamics, and the modern technique of optical levitation. The apparatus we have presented can be used to study various physical effects. For example, as a next step, we aim to investigate the whispering gallery modes that can occur in this type of motion.

ACKNOWLEDGMENTS

This work was supported by grants from the Swedish Research Council and from the Knut and Alice Wallenberg Foundation for the project Bottlenecks for particle growth in turbulent aerosols (Dnr. KAW 2014.0048), J.T.M. and R.C.-T. acknowledge support from the Linneaus-Palme foundation, and O.I. acknowledges support from Sannarpsgymnasiet, Halmstad. Finally, the authors appreciate the comments provided by Professor David J. Pegg during the writing of this manuscript.

APPENDIX: LIST OF EXPERIMENTAL COMPONENTS

- **Laser** GEM-532 from Laser Quantum. Wavelength 532 nm and power 50 mW to 2 W. Approximate cost: $10000.
- **Droplet Dispenser** Bent steel capillary (No. A010-002) and control unit multi-dose 2 (No. A020-301). Approximate cost: $5000.
- **Vacuum Pump** Pfiffer vacuum rotary vane pump. Model Duo 5M. Approximate cost: $1500.
- **PSD** Sitek Electro-Optics AB one dimensional PSD, area $20 \cdot 3$ mm. Part No: S1-0006. Approximate cost: $120.
- **Voltage Amplifier** Kepco Model BOP1000M. Approximate cost: $1000.
- **Trapping Cell** The cell is fabricated in our technical department to an unknown cost.
- **Optics** Additional optics. We use two mirrors to direct the laser and three lenses to focus the laser and to image the droplet.

- **Function Generator** Leader LFG-1300. Approximate cost: $150 (used).
- **Data Acquisition Device**, National Instruments NI BNC-2110, PCIe-6321 and SHC68-68-EPM cable. Approximate cost: $1200 (used).

[a]Electronic mail: javier.marmolejo@physics.gu.se
[b]On sabbatical leave at the Theoretische Chemie, Physikalisch-Chemisches Institut, Universität Heidelberg, INF 229, 69120 Heidelberg, Germany.

[1]Frank Oppenheimer, "Forced harmonic oscillator," Am. J. Phys. **31**, 13–24 (1963).
[2]Francis J. McCormack, "Smooth transitions between the three damping cases for the harmonic oscillator," Am. J. Phys. **63**, 1151 (1995).
[3]Dennis Ugolini, Hanna Rafferty, Max Winter, Carsten Rockstuhl, and Antje Bergmann, "LIGO analogy lab—A set of undergraduate lab experiments to demonstrate some principles of gravitational wave detection," Am. J. Phys. **87**, 44–56 (2019).
[4]Marcello Carla and Samuele Straulino, "Measurements on a guitar string as an example of a physical nonlinear driven oscillator," Am. J. Phys. **85**, 587–595 (2017).
[5]Patrick Shea, Brandon P. van Zyl, and Rajat K. Bhaduri, "The two-body problem of ultra-cold atoms in a harmonic trap," Am. J. Phys. **77**, 511–515 (2009).
[6]Phillip Gould, "Laser cooling of atoms to the Doppler limit," Am. J. Phys. **65**, 1120–1123 (1997).
[7]Michael J. Ruiz, "The human body's response to glucose and three physical models," Am. J. Phys. **55**, 641–645 (1987).
[8]R. Hauko, D. Andreevski, D. Paul, M. Sterk, and R. Repnik, "Teaching of the harmonic oscillator damped by a constant force: The use of analogy and experiments," Am. J. Phys. **86**, 657–662 (2018).
[9]Christopher C. Jones, "A mechanical resonance apparatus for undergraduate laboratories," Am. J. Phys. **63**, 232–236 (1995).
[10]David Faiman and Archibald W. Hendry, "Electromagnetic decays of baryon resonances in the harmonic-oscillator model," Phys. Rev. **180**, 1572–1577 (1969).
[11]Wenhua Zhang and Kimberly L. Turner, "Application of parametric resonance amplification in a single-crystal silicon micro-oscillator based mass sensor," Sens. Actuators, A **122**, 23–30 (2005).
[12]Kenneth G. Holt, Joseph Hamill, and Robert O. Andres, "Predicting the minimal energy costs of human walking," Med. Sci. Sports Exercise **23**, 491–498 (1991).
[13]M. Alonso and E. J. Finn, *Fundamental University Physics, Volume I, Mechanics*, 1st ed. (Addison-Wesley Publishing Company, Reading, MA, 1976).
[14]D. Halliday, R. Resnick, and J. Walker, *Principles of Physics*, 9th ed. (Wiley, Hoboken, NJ, 2011).
[15]R. D. Knight, *Physics for Scientists and Engineers: A Strategic Approach with Modern Physics*, 1st ed. (Pearson Education, San Francisco, CA, 2016).
[16]A. Giambattista, B. M. C. Richardson, and R. C. Richardson, *College Physics*, 1st ed. (McGraw-Hill Higher Education, New York, NY, 2007).
[17]J. C. Zamora, F. Fajardo, and J.—A. Rodríguez, "Oscillator experiments with periods between the simple pendulum and a rigid rod," Am. J. Phys. **77**, 169–172 (2009).
[18]D. Kharkongor and Mangal C. Mahato, "Resonance oscillation of a damped driven simple pendulum," Eur. J. Phys. **39**, 065002 (2018).
[19]A. Ashkin, "History of optical trapping and manipulation of small-neutral particle, atoms, and molecules," IEEE J. Sel. Top. Quantum Electron. **6**, 841–856 (2000).
[20]A. Ashkin and J. M. Dziedzic, "Optical levitation by radiation pressure," Appl. Phys. Lett. **19**, 283–285 (1971).
[21]Stephen P. Smith, Sameer R. Bhalotra, Anne L. Brody, Benjamin L. Brown, Edward K. Boyda, and Mara Prentiss, "Inexpensive optical tweezers for undergraduate laboratories," Am. J. Phys. **67**, 26–35 (1999).
[22]John Bechhoefer and Scott Wilson, "Faster, cheaper, safer optical tweezers for the undergraduate laboratory," Am. J. Phys. **70**, 393–400 (2002).
[23]M. S. Rocha, "Optical tweezers for undergraduates: Theoretical analysis and experiments," Am. J. Phys. **77**, 704–712 (2009).
[24]D. C. Appleyard, K. Y. Vandermeulen, H. Lee, and M. J. Lang, "Optical trapping for undergraduates," Am. J. Phys. **75**, 5–14 (2007).
[25]Oscar Isaksson, Magnus Karlsteen, Mats Rostedt, and Dag Hanstorp, "An optical levitation system for a physics teaching laboratory," Am. J. Phys. **86**, 135–142 (2018).
[26]J. Mas, A. Farre, J. Cuadros, I. Juvells, and A. Carnicer, "Understanding optical trapping phenomena: A simulation for undergraduates," IEEE Trans. Educ. **54**, 133–140 (2011).
[27]A. Ashkin and J. M. Dziedzic, "Optical levitation in high vacuum," Appl. Phys. Lett. **28**, 333–335 (1976).
[28]A treatment with equivalent results can be found in Ref. 13. Otherwise, it is easy to derive Eqs. (5) and (6) by plugging Eq. (4) into Eq. (1). For Eq. (5) make $t = 0$ and for Eq. (6) $t = \pi/2\omega$ and $\alpha' = \alpha + (\pi/2)$.
[29]A. Ashkin, "Forces of a single-beam gradient laser trap on a dielectric sphere in the ray optics regime," Biophys. J. **61**, 569–582 (1992).
[30]E. Hetch, *Optics*, 4th ed. (Addison-Wesley, San Francisco, CA, 2002).
[31]Thomas R. Lettieri, Wilhelmina D. Jenkins, and Dennis A. Swyt, "Sizing of individual optically levitated evaporating droplets by measurement of resonances in the polarization ratio," Appl. Opt. **20**, 2799–2805 (1981).
[32]A. Chiasera, Y. Dumeige, P. Féron, M. Ferrari, Y. Jestin, G. Nunzi Conti, S. Pelli, S. Soria, and G. C. Righini, "Spherical whispering-gallery-mode microresonators," Laser Photonics Rev. **4**, 457–482 (2010).